Progress In Electromagnetics Research, Vol. 153, 93–102, 2015

Equivalent-Circuit Models for Efficient Transmission and Dispersion Analyses of Multi-State Periodic Structures

Ladislau Matekovits[1, *], Dushmantha N. Thalakotuna[2], Karu P. Esselle[2], Stuart G. Hay[3], and Michale Heimlich[2]

Abstract—An equivalent-circuit model for a reconfigurable unit cell is proposed. This circuit model facilitates fast prediction of scattering parameters and dispersion analyses of a reconfigurable periodic structure. The cutoff frequencies obtained using equivalent-circuit models are in excellent agreement with those from measurements and full-wave numerical simulations. The proposed circuit model is then modified to include non-ideal, commercial RF FET switches. The effect of such a switch in each state, On or Off, is modeled by a frequency-dependant impedance, derived from the scattering parameters of the switch. The proposed technique can be used to analyze a reconfigurable periodic structure with any type of switches. For the structure with 24 unit cells considered here, the equivalent circuit model is about five orders of magnitude faster than full-wave simulations.

1. INTRODUCTION

Microwave periodic structures have gained increasing attention during last few decades due to their interesting propagation characteristics [1, 2]. The upper and lower limits of the bandgap (or stopband) of such a microwave structure depend on the lattice structure, periodicity (lattice constant) and the geometrical configuration of the unit cell. In conventional microwave periodic structures all these are fixed and consequently the bandgap is fixed as well. This prevents their direct use in certain advanced applications, where tunability or reconfigurability is required. The use of active switches such as diodes, Field Effect Transistors (FET) or microelectromechanical systems (MEMS) inside the unit cells provides a way of controlling the lattice structure of a unit cell. This concept has been used to transform passive periodic structures to active structures that can provide reconfigurability [3].

Although a reconfigurable periodic structure can be accurately characterized through measurements, this approach can be expensive and time consuming as it requires prototype fabrications. Therefore full-wave numerical simulations are commonly used for their design and analysis [4–6]. In general, full-wave numerical simulations of passive periodic structures are relatively less demanding since they usually require only one simulation run. In contrast, reconfigurable periodic structures require many simulation runs, one for each configuration. This demands extensive computational resources and time, especially when the unit cell itself is geometrically complex.

An equivalent-circuit model representation is an alternative to full-wave numerical techniques [7–11]. However equivalent-circuit models in general are limited in their ability to represent the circuit response in a wide frequency range. This is mainly due to effects of higher-order modes that are usually not accounted for in circuit representations. Despite this limitation, equivalent-circuit models are very efficient and fast to predict the behavior of periodic structures specially in the preliminary stages of the design. Further they can be used as an efficient tool to study the sensitivity of the bandgap to various parameters of the unit cell.

Received 8 July 2015, Accepted 29 September 2015, Scheduled 22 October 2015

* Corresponding author: Ladislau Matekovits (ladislau.matekovits@polito.it).

[1] Dipartimento di Elettronica e Telecomunicazioni, Politecnico di Torino, 24 C.so Duca degli Abruzzi, Torino 10129, Italy.

[2] Department of Engineering, Macquarie University, Sydney 2109, Australia. [3] CSIRO Data61, Marsfield, NSW 2122, Australia.

In this paper we present an equivalent-circuit model for a unit cell in a reconfigurable periodic structure. Then we apply the model to compute the dispersion diagrams and transmission parameters of a reconfigurable microwave filter. The unit cell in this design has two main states. The complete periodic structure may contain a few dozen of such unit cells. The periodicity in the structure can be changed by varying the state of individual unit cells according to a periodic state pattern. Each possible state of the unit cell is represented by a circuit model and this enables us to represent the complete periodic structure by a network of circuit segments, each representing a unit cell. This circuit topology allows us to predict efficiently the first passband and stopband of the periodic structure for all possible (periodic and non-periodic) state patterns. Further, it provides an extremely efficient way to compute dispersion characteristics of the periodic structure for all periodic state patterns. This has proven extremely useful in analyzing dispersion behavior of certain periodic state patterns when commercial eigen-mode solvers fail to converge to the required accuracy.

The equivalent-circuit model is then modified to accurately represent the non-ideal and dispersive nature of a commercially-available FET switch package, using its frequency-dependent scattering parameters. The proposed method is verified with full-wave numerical simulations and experiments. It is extremely fast in predicting the scattering parameters and dispersion diagrams of reconfigurable periodic structures with switches, compared to full-wave numerical simulations. To the best of our knowledge, such a fast technique based on equivalent-circuit models has not been developed before to analyze reconfigurable periodic structures with switches.

2. CONFIGURATION

The periodic structure modeled here is a microstrip line with additional metallic patches embedded inside the substrate along the transmission line as shown in Fig. 1. The layer of rectangular printed patches is located 13 mils (h_2) beneath the microstrip as shown in Fig. 1(b). The ground plane is at the bottom of the substrate. The substrate thickness between the patches and ground plane is 60 mils (h_1). In the current example the same dielectric material, Nelco N4000 13SI ($\epsilon_r = 3.4$ and $\tan\delta = 0.01$), is used as the substrate above and below the patches but it's also possible to use two different dielectrics for these two regions as discussed in previous works [12–15]. The complete structure contains 24 patches. Each patch can be selectively grounded using two discrete FET switches placed at the bottom ground-plane. The two vias at the ends of a patch goes through the substrate to the ground-plane level and connects to the ground through the switches. In other words, a unit cell contains two switches residing between the ground and vias as shown in Fig. 1(b). This pair of switches are operated together to connect the patch to, or disconnect it from the ground. The "On" state of the switch grounds the patch while the "Off" state lets the metal patch float. The "On" and "Off" switch states are represented by State "1" and State "0" hereafter. Two standard SMA connectors are provided at the two ends of the periodic structure.

The proposed architecture to reconfigure the state of each unit cell provides the flexibility to impose different periodic and aperiodic loading patterns along the microstrip line by changing the effective position of the ground below the microstrip. When this loading is imposed in a periodic manner the circuit becomes an electromagnetic bandgap structure. Therefore the stopband can be altered by changing the state pattern along the structure.

In this work the "On" and "Off" state of the switch is initially modeled assuming ideal conditions, as a short circuit and a capacitive gap between the vias and ground, respectively. Then a more accurate model, based on scattering parameters, is introduced for non-ideal commercial FET switches.

3. CIRCUIT MODEL

3.1. Circuit Model of the Unit Cell

The middle segment of the microstrip line in each unit cell is directly above the patch. This segment is modeled as a lumped equivalent circuit to a microstrip line [16], with the patch acting as the ground plane for the microstrip. As shown in Fig. 2 this segment is represented by inductance L_{ms} and two capacitances $C_{mspatch}$. The other two segments are modeled as microstrip lines with the conventional

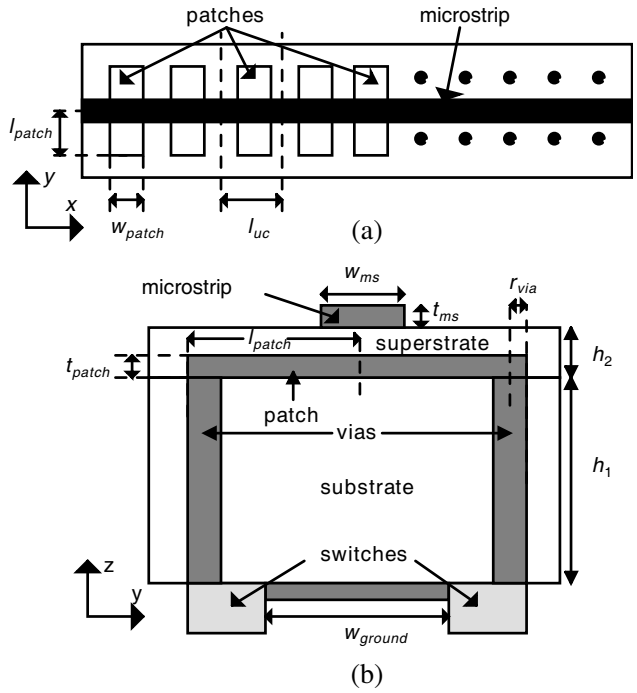

Figure 1. (a) A top view of both microstrip and patch layers. These layers are not in the same plane. The dots on the sides of the microstrip denotes the repetition of patches along the microstrip line. (b) Side view of a unit cell. The parameter values are given in Table A1 in Appendix A.

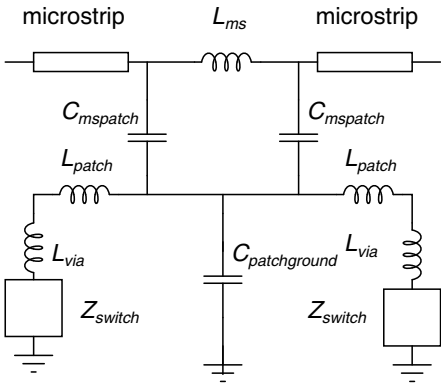

Figure 2. Circuit representation of a reconfigurable unit cell with active switches.

bottom ground plane. The patch is represented by two lumped inductors L_{patch} and a capacitance $C_{patchground}$ to the ground. The vias are modeled as inductances L_{via} between the patch and ground. The values of all these lumped circuit elements can be calculated from unit cell dimensions using the closed-form formulas given in Appendix A. The impedance z_{switch} between each via and the ground represents the switch. It indeed has two values, depending on the state of the switch. In Section 6, we outline how these values can be estimated for a commercial non-ideal FET switch from its s-parameters. In Section 4 and 5, z_{switch} of a unit cell in state "1" is set to zero assuming ideal switch "On" condition. In State "0", vias are isolated from the ground by a gap; hence z_{switch} can be calculated from a very low gap capacitance $C_{viaground}$ or simply replaced by an open circuit, again assuming an ideal switch.

3.2. Circuit Model of the Complete Periodic Structure

The complete equivalent-circuit, for the periodic structure containing 24 unit cells, is obtained by cascading unit cell circuit models. The unit cell states "1" and "0", can be combined to create arbitrary state patterns, some of these are periodic. For example "...1010..." periodic state pattern can be created by cascading "1" and "0" unit cells alternatively. Each of these complete periodic state patterns is based on a unique repetitive pattern. This unique repetitive pattern in its simplest non-repetitive form is defined as a macro cell. For example "10" is the macro cell in the "...1010..." periodic state pattern.

4. TRANSMISSION ANALYSIS

The derived lumped element values listed in Table A2 in Appendix A were used in AWR circuit simulator to calculate the transmission of the complete periodic structure for various state patterns. The results

for the "..11.." state pattern are compared with measurements and full-wave numerical results (obtained from CST MWS) in Fig. 3. The experimental passive periodic structure represents ideal switches as close as possible, with a solder dot closing the gap between the via and ground to represent the State "1". The gap was left open to represent State "0" in some experiments.

The circuit model calculated the scattering parameters very well up to the end of the first stopband. Our circuit model approximations are valid as long as the guided wavelength λ_g is much larger than the lumped elements. Within the first passband all the lumped element dimensions are at least one tenth of λ_g or less. However around 6 GHz that is the onset of the second passband the largest circuit element length is greater than $0.2\lambda_g$. This leads to inaccuracies in predicting the behavior in second passband. In addition, the circuit representation for the fundamental mode is different from the circuit representations of higher-order modes. This leads to deviations between the insertion loss values obtained from the circuit model and measurements after the upper limit of the stopband.

The equivalent-circuit model was further verified through a parametric study. Fig. 4 shows a comparison between CST full-wave numerical results and circuit model results for different substrate and superstrate permittivity values. The calculated -10 dB stopband values from equivalent circuit model are within 5% of the corresponding full-wave numerical simulation values.

The same technique was used to derive transmission parameters of few other important state patterns such as "..10.." and "..00..". The lower (f_L) and higher (f_H) limits of the stopband obtained from measurements, full-wave numerical simulations and circuit simulations are compared in Table 1 for these state patterns. The full-wave numerical simulations were carried out using a distributed computing setup consisting of two computers, each with a core i5 2.89 GHz processor and 4 GB RAM. The total

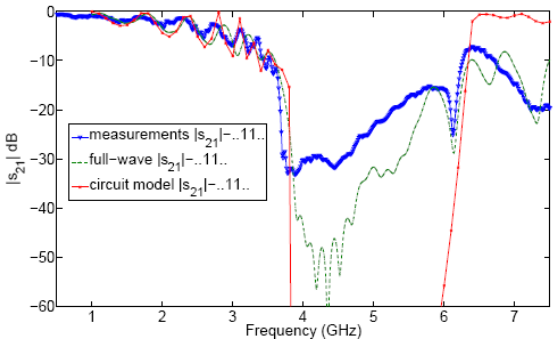

Figure 3. Comparison of the measured and simulated $|s_{21}|$ for the "..11.." state pattern. Circuit simulation time: 0.65 seconds, CST simulation time with -50 dB steady state level accuracy: 13 hours 55 minutes 49 seconds.

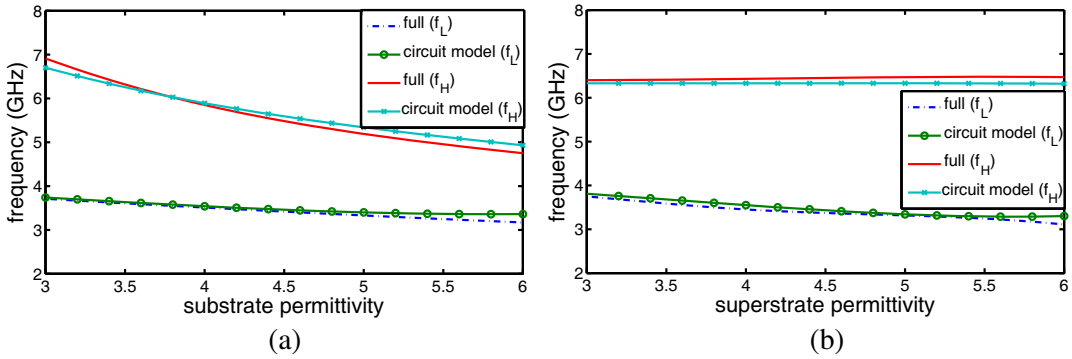

Figure 4. Comparison of lower and higher stopband limits with the change in (a) substrate permittivity, (b) superstrate permittivity for the "..11.." state pattern obtained through full-wave numerical simulations and the equivalent-circuit model.

Table 1. Comparison of the results from measurements, full-wave numerical analysis and circuit models for three state patterns.

	..11..			..10..			..00..		
	Full wave	Circuit model	Measure -ments	Full wave	Circuit model	Measure -ments	Full wave	Circuit model	Measure -ments
f_L GHz	3.63	3.66	3.56	3.75	3.7	3.53	No bandgap	No bandgap	No bandgap
f_H GHz	6.43	6.33	6.24	5.30	5.25	5.19	No bandgap	No bandgap	No bandgap
Simulation time	13 h 55 m49 s	0.65 s	N/A	22 h 11 m52 s	0.65 s	N/A	3 h 22 m38 s	0.65 s	N/A

simulation time for the "...11..." periodic pattern was 13 hours 55 minutes 49 seconds for a -50 dB level accuracy in CST transient solver as opposed to 0.65 seconds for the circuit simulator on a single computer with a core 2 duo 3 GHz processor and 4 GB RAM. It is clear that the circuit simulation is extremely efficient in computing the scattering parameters of a reconfigurable periodic structure.

5. DISPERSION ANALYSIS

Dispersion analysis reveals the relationship between the propagation constant k and frequency f of an infinite periodic structure. They are still useful in practical applications because a finite periodic structure with sufficiently large number of unit cells can be approximated by an infinite periodic structure. Usually full-wave eigen-mode solvers are employed for dispersion analysis. However popular commercial eigen-mode solvers can be extremely time consuming and therefore inefficient when one needs to analyze dispersion of a complex reconfigurable structure for several configurations. As an alternative, the equivalent-circuit models, derived in Section 3 are used here for efficient dispersion analysis of infinite reconfigurable structures.

5.1. *ABCD* Matrix of a Unit Cell

The propagation constant γ of an infinite periodic structure can be derived from the $ABCD$ transmission matrix of a unit cell [17] as

$$\gamma = \frac{1}{d}\cosh^{-1}\left(\frac{A+D}{2}\right) \tag{1}$$

The term d denotes the length of the unit cell and A and D are the diagonal elements of $ABCD$ transmission matrix of the unit cell. The propagation constant contains both the attenuation constant (α) and the phase constant (β), which are useful to describe the dispersion behavior of the periodic structure. The unit cell considered in this research can be viewed as a cascade of three segments namely a microstrip line, a lumped-element segment and a microstrip line, as shown in Figs. 2 and 5. Therefore the complete unit cell matrix, $ABCD_{uc}$, can be calculated as the product of $ABCD$ matrices of the individual segments:

$$ABCD_{uc} = ABCD_{ms} \times ABCD_{cct} \times ABCD_{ms} \tag{2}$$

The $ABCD$ matrix of the microstrip segments are given by

$$ABCD_{ms} = \begin{bmatrix} \cos\beta l_{ms} & jZ_0 \sin\beta l_{ms} \\ jY_0 \sin\beta l_{ms} & \cos\beta l_{ms} \end{bmatrix} \tag{3}$$

In order to obtain $ABCD_{cct}$, the network of lumped elements in Fig. 2 is transformed to the T-network topology shown in Fig. 5. This leads to closed-form expressions for the T-network impedance

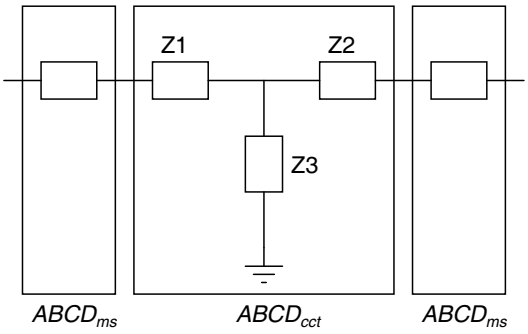

Figure 5. The $ABCD$ matrix of a unit cell is calculated by multiplying $ABCD$ matrices of three parts.

parameters, Z_1, $Z_2(= Z_1)$ and Z_3 shown in Fig. 5. Then, the $ABCD$ matrix of the lumped elements is given by

$$ABCD_{cct} = \begin{bmatrix} 1 + \dfrac{Z_1}{Z_3} & Z_1 + Z_2 + \dfrac{Z_1 Z_2}{Z_3} \\ \dfrac{1}{Z_3} & 1 + \dfrac{Z_2}{Z_3} \end{bmatrix} \tag{4}$$

The α and β for the "..11.." periodic state pattern obtained using the equivalent-circuit model by combining Eqs. (1) to (4) are plotted in Fig. 6. It can be observed that the attenuation constant α remains zero in the passbands since transmission matrix of the circuit does not account for any conductor losses. The lower limit f_L and higher limit f_H of the stopband for the "...11..." state pattern, obtained this way from the equivalent-circuit model, are 3.84 GHz and 6.4 GHz, respectively. They agree very well with the results from the CST eigen-mode solver, which are 3.85 GHz and 6.2 GHz, respectively. As shown in Fig. 6, the CST eigen-mode solver results are in close agreement with the circuit model results up to the start of the second passband. The deviation above the higher cut off is due to inaccurate circuit representation of the first higher-order mode. In the stopband (3.92 GHz–6.4 GHz) attenuation constant is very large due to the electromagnetic bandgap.

Although the dispersion analyses assume infinite periodic structures, the lower and upper limits of the stopband obtained from dispersion diagram for "..11.." state pattern agree closely with the corresponding f_L and f_H frequencies, 3.56 GHz and 6.24 GHz, for the finite twenty-four unit cell structure obtained in Section 4 from measurements (see Table 1).

The CST eigen-mode solutions took in total 8 hours 42 minutes and 52 seconds to compute the wavenumbers for "...11..." state pattern in a distributed computing setup that used 8 computers each with one Intel core i5 2.89 GHz processor and 4 GB of RAM. Alternatively the circuit model method took only 1.183 seconds in a computer with Pentium core 2 Duo 3 GHz processor and 4 GB of RAM.

5.2. *ABCD* Matrix of a Macro Cell

Since a macro cell is composed of two or more unit cells, the complete transmission matrix of the macro cell is given by the product of transmission matrices of individual unit cells:

$$ABCD_{mc} = \prod_{k=1}^{p} ABCD_{uc_n} \tag{5}$$

where p is the number of unit cells in the macro cell and $n \in \{0, 1\}$ the state of the kth unit cell. The dispersion diagram for the "...10..." state pattern obtained using the equivalent-circuit model is shown in Fig. 6. The CST eigen-mode solver failed to converge to the required accuracy for some phase points for this "10" macro cell. With the circuit model, it was possible to calculate the dispersion diagram for "..10.." periodic state pattern in 1.183 seconds in a computer with Pentium core 2 Duo 3 GHz processor and 4 GB of RAM. The lower and higher limits of the stopband in "..10.." pattern, obtained from this dispersion analysis, are 3.7 GHz and 5.3 GHz, respectively. They agree closely with the stopband limits

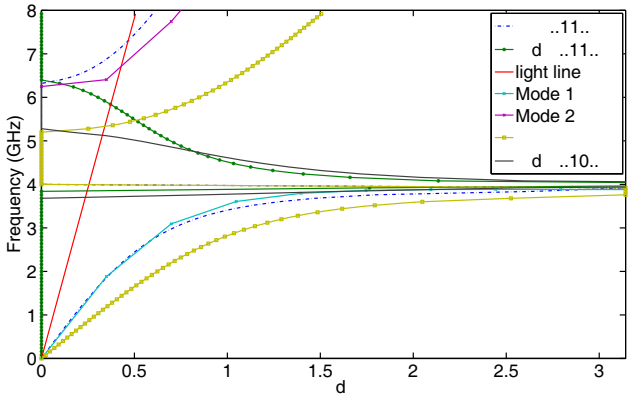

Figure 6. Dispersion diagrams for "..11.." and "..10.." state patterns. Simulation time for state "..11.." unit cell in CST eigen mode solver: 8 hours 42 minutes and 52 seconds using distributed computing; CST eigen-mode solver failed to achieve the required accuracy when computing the dispersion diagram for "..10.." pattern; circuit model simulation time for each state pattern: 1.183 seconds.

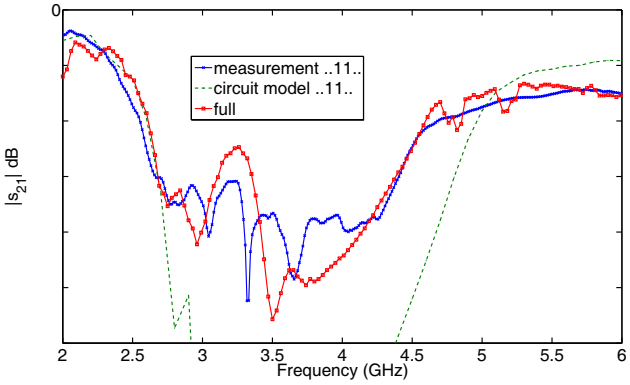

Figure 7. $|s_{21}|$ for "..11.." periodic state pattern obtained with non-ideal models for RF switches.

obtained in Section 4 for the finite structure from measurements, that are 3.53 GHz and 5.19 GHz (see Table 1).

6. PERIODIC STRUCTURES WITH NON-IDEAL RF SWITCHES

In this section we consider actual RF switches such as packaged GaAs pHEMT switches. Their effective impedance between two RF ports (z_{switch} in Fig. 2) is frequency dependent. This is now represented by $Z(f)_{switch}$. Obviously this impedance also changes significantly when the switch state is changed between "On" and "Off".

In the current study, MACOM MASW-007921 Single Pole Double Throw (SPDT) switch is considered as the RF switch. Its two-port impedance matrix was computed for each state, from the manufacturer-provided scattering parameters of the switch, using the standard transformations given in [18]. Then its lumped equivalent switch impedance $Z(f)_{switch}$ was determined for each state of the switch from the two-port impedance matrices by.

$$Z(f)_{switch} = Z(f)_{11} - Z(f)_{12} - Z(f)_{21} + Z(f)_{22} \tag{6}$$

6.1. Transmission Analysis

The transmission through the 24 unit cell periodic structure for "...11..." state pattern, obtained with these frequency-dependent impedance models for the RF switches, is plotted in Fig. 7. These equivalent-circuit model results agree very well with the results from the full-wave CST MWS transient solver and experiments in the first passband as shown in the same figure. The cut-off frequencies, f_L and f_H (defined at -20 dB level) from equivalent-circuit model are 2.63 GHz and 4.72 GHz and the corresponding values from measurements are 2.55 GHz and 4.67 GHz, respectively. Similarly for state pattern "..10..", equivalent circuit predicts 2.72 GHz (f_L) and 5.95 GHz (f_H) while corresponding values from measurements are 2.54 GHz and 6.23 GHz. With the introduction of FET switches in the patch to ground paths, the bandgap shifts down in frequency, as noted in [19]. The increase in transmission losses is due to the losses introduced by the switches.

The full-wave simulation results shown in Fig. 7 also utilized the manufacturer-provided scattering parameters for the RF switches. These full-wave simulation were done in a distributed setup using 12

computers each with one core i5 2.89 GHz processor and 4 GB RAM. The total simulation time was 5 days 7 hours 56 minutes and 56 seconds. In contrast, the circuit simulator took only 0.02 seconds in a Pentium core 2 Duo 3 GHz processor with 4 GB of RAM. Yet the agreement between two results is reasonable at lower frequencies where the equivalent-circuit model is valid. As in the passive case, the equivalent-circuit model over estimate the attenuation in the bandgap and become inaccurate in the second passband.

6.2. Dispersion Analysis

The $Z(f)_{switch}$ derived from Eq. (6) is used to calculate the dispersion curve for the periodic structure with MACOM MASW-007921 RF switches. The attenuation constant derived for "..11.." state pattern shows sudden changes at 2.5 GHz and 4.9 GHz. These frequencies closely agree with the stopband limits determined from measured transmission at -20 dB level, which are 2.55 GHz and 4.67 GHz respectively. Similarly attenuation constant change rapidly at, 2.5 GHz and 6.3 GHz for "..10.." state pattern. The corresponding -20 dB measured stopband limits are 2.54 GHz and 6.23 GHz. Therefore dispersion analysis of an equivalent-circuit model can be used to predict the position of the stopband efficiently with a reasonable accuracy when the non-ideal nature of the RF switch is accounted.

7. CONCLUSION

The use of popular full-wave software packages for the transmission and dispersion analyses of reconfigurable periodic structures can lead to large computing times (in the order of days) even in distributed computing environments. The proposed equivalent-circuit approach is an extremely efficient and reasonably accurate way to calculate the transmission parameters of a reconfigurable periodic structure for all possible periodic and aperiodic switching patterns. It is also robust and extremely efficient for dispersion analysis of such structures. With the proposed equivalent-circuit models, both types of analysis take only a fraction of a second in an ordinary PC. The lumped-circuit element values in the proposed models can be calculated from the physical geometry parameters of the unit cell using simple closed-form expressions. The refined equivalent-circuit model accounts for the non-ideal, dispersive behavior of commercially-available switches.

The proposed equivalent-circuit model is verified through measurements and full-wave simulations on a periodic structure with 24 unit cells. It accurately predicts the edges of the stopband for a range of dielectric constants. The results obtained with the current equivalent circuit model is more accurate in the first passband in which the fundamental microstrip mode dominates. It becomes less accurate when higher-order modes appear because some element values in the current model has been derived by assuming fundamental TEM mode. Nevertheless, fast simulation time makes this equivalent circuit model extremely useful in initial design stages. Although the focus of this paper is on periodic reconfigurable structures, the proposed approach is equally applicable for non-periodic reconfigurable structures composed of similar, modified-microstrip segments.

APPENDIX A. CALCULATION OF CIRCUIT ELEMENTS

The lumped element values, L_{ms} and $C_{mspatch}$, can be calculated from [16]:

$$L_{ms}(\text{nH}) = 2 \times 10^{-4} w_{patch} \left[\ln\left(\frac{w_{patch}}{w_{ms} + t_{ms}} \right) + 1.193 + \frac{w_{ms} + t_{ms}}{3 w_{patch}} \right] K_g \tag{A1}$$

$$C_{mspatch}(\text{pF}) = 16.67 \times 10^{-4} w_{patch} \sqrt{\varepsilon'_{re}} / Z_0 + C_f \tag{A2}$$

where w_{patch}, w_{ms}, t_{ms}, ε'_{re}, Z_0 and K_g are the width of the patch, width of the microstrip line, thickness of the microstrip line, effective dielectric constant, characteristic impedance of the microstrip line and a term accounted for the presence of a ground plane [16], respectively. The dimensions in Eqs. (A1) and (A2) are in micrometers. The effective dielectric constant ε'_{re} is modified to account the effect of additional dielectric prepeg layer, which is required for the fabrication. The fringe capacitance C_f between the microstrip and patch is calculated using the formulas in [20].

Table A1. parameter values.

Parameter	Value
w_{ms}	50 mils
t_{ms}	0.5 mils
h_1	60 mils
h_2	13 mils
r_{via}	8.84 mils
w_{patch}	80 mils
l_{patch}	225 mils
t_{patch}	0.5 mils
w_{ground}	250 mils
l_{uc}	120 mils
ε'_{re}	3.67
ϵ_r	3.4

Table A2. Lumped element circuit values.

Lumped element	Derived value
L_{ms}	0.2837 nH
$C_{mspatch}$	0.3093 pF
$C_{patchground}$	0.3362 pF
L_{via}	0.609 nH
L_{patch}	2.628 nH
C_f	0.068 pF
C_f^{pg}	0.081 nH
$C_{viaground}$	0.001 pF

The inductance of a via and the patch is approximated from the closed form formulas in [21]:

$$L_{via}(\text{nH}) = 2\times 10^5 \left[h_1 \ln\left(\frac{h_1+\sqrt{r_{via}^2+h_1^2}}{r_{via}}\right)\right] + 2\times 10^5\left[\frac{h_1}{4}+r_{via}-\sqrt{r_{via}^2+h_1^2}\right] \quad \text{(A3)}$$

$$L_{patch}(\text{nH}) = 2\times 10^2 l_{patch}\left[\ln\frac{2l_{patch}}{\chi}-1+\frac{\chi}{l_{patch}}\right] \quad \text{(A4)}$$

where

$$\chi = 0.2235(t_{patch}+w_{patch}) \quad \text{(A5)}$$

The capacitance between the patch and ground is calculated by,

$$C_{patchground}(F) = \frac{\epsilon_0\epsilon_r l_{patch} w_{patch}}{h_1} + C_f^{pg} \quad \text{(A6)}$$

The terms l_{patch}, h_1, r_{via}, ϵ_0, ϵ_r and t_{patch} denote half the length of the patch, thickness of the substrate from ground to patch, radius of the via, permittivity of air, substrate dielectric constant and thickness of the patch. The fringe capacitance C_f^{pg} [20] between the patch and ground is accounted for in $C_{patchground}$.

The derived lumped elements values are listed in Table A2 and the corresponding parameter values are given in Table A1.

REFERENCES

1. Eleftheriades, G., A. Iyer, and P. Kremer, "Planar negative refractive index media using periodically L-C loaded transmission lines," *IEEE Trans. on Microwave Theory and Tech.*, Vol. 50, No. 12, 2702–2712, Dec. 2002.
2. Sor, J., Y. Qian, and T. Itoh, "Miniature low-loss CPW periodic structures for filter applications," *IEEE Trans. on Microwave Theory and Tech.*, Vol. 49, No. 12, 2336–2341, Dec. 2001.
3. Karim, M., A.-Q. Liu, A. Alphones, and A. Yu, "A reconfigurable micromachined switching filter using periodic structures," *IEEE Trans. on Microwave Theory and Tech.*, Vol. 55, No. 6, 1154–1162, Jun. 2007.
4. Baccarelli, P., C. Di Nallo, S. Paulotto, and D. Jackson, "A full-wave numerical approach for modal analysis of 1-D periodic microstrip structures," *IEEE Trans. on Microwave Theory and Tech.*, Vol. 54, No. 4, 1350–1362, Jun. 2006.

5. Lee, H. and J. Kim, "Unit cell approach to full-wave analysis of meander delay line using FDTD periodic structure modeling method," *IEEE Trans. on Advanced Packaging*, Vol. 25, No. 2, 215–222, May 2002.
6. Matekovits, L., G. Vecchi, M. Bercigli, and M. Bandinelli, "Efficient numerical analysis of large planar high impedance surface by the synthetic function expansion (SFX) technique," *Microwave and Optical Technology Letters*, Vol. 51, 2763–2769, Nov. 2009.
7. Shahparnia, S. and O. Ramahi, "A simple and effective model for electromagnetic bandgap structures embedded in printed circuit boards," *Microwave and Wireless Components Letters*, Vol. 15, No. 10, 621–623, Oct. 2005.
8. Rogers, S., "Electromagnetic-bandgap layers for broad-band suppression of TEM modes in power planes," *IEEE Trans. on Microwave Theory and Tech.*, Vol. 53, No. 8, 2495–2505, Aug. 2005.
9. Mohajer-Iravani, B. and O. Ramahi, "Wideband circuit model for planar EBG structures," *IEEE Trans. on Advanced Packaging*, Vol. 33, No. 1, 169–179, Feb. 2010.
10. Sievenpiper, D., L. Zhang, R. Broas, N. Alexopolous, and E. Yablonovitch, "High-impedance electromagnetic surfaces with a forbidden frequency band," *IEEE Trans. on Microwave Theory and Tech.*, Vol. 47, No. 11, 2059–2074, Nov. 1999.
11. Gil, I., J. Bonache, J. Garcia-Garcia, and F. Martin, "Tunable metamaterial transmission lines based on varactor-loaded split-ring resonators," *IEEE Trans. on Microwave Theory and Tech.*, Vol. 54, No. 6, 2665–2674, Jun. 2006.
12. Matekovits, L., D. Thalakotuna, M. Heimlich, and K. Esselle, "Investigation on FET switch integration techniques for a tunable microwave periodic structure," *Proc. International Workshop on Antenna Technology (iWAT)*, 44–47, Mar. 2012.
13. Matekovits, L., D. Thalakotuna, M. Heimlich, and K. P. Esselle, "Wideband matching of a tunable periodic structure in GaAs technology," *Proc. International Workshop on Antenna Technology (iWAT)*, 376–379, Mar. 2011.
14. Thalakotuna, D., L. Matekovits, K. Esselle, and M. Heimlich, "Dynamic tuning of electromagnetic bandgap," *Proc. of the 5th European Conference on Antennas and Propagation*, 1065–1067, Apr. 2011.
15. Thalakotuna, D., L. Matekovits, K. Esselle, and M. Heimlich, "Effect of active device insertion losses on the electromagnetic bandgap characteristics of a tunable 1D periodic structure in the S band," *Proc. 2011 IEEE International Symposium on Antennas and Propagation*, 1808–1811, Jul. 2011.
16. Bahl, I. J., *Lumped Elements for RF and Microwave Circuits*, Artech House, 2003.
17. Collin, R. E., *Foundation of Microwave Engineering*, 1st Edition, McGrawHill, New York, 1966.
18. Pozar, D. M., *Microwave Engineering*, John Wiley and Sons, 1998.
19. Thalakotuna, D., L. Matekovits, M. Heimlich, K. P. Esselle, and S. G. Hay, "Active switching devices in a tunable ebg structure: Placement strategies and modelling," *Journal of Electromagnetic Waves and Applications*, Vol. 25, Nos. 11–12, 1740–1751, 2011.
20. Hong, J.-S. and M. J. Lancaster, *Microstrip Filters for RF/Microwave Applications*, John Wiley and Sons, 2001.
21. Rosa, E., "The self and mutual inductances of linear conductors," *Bulletin of the Bureau of Standards*, Vol. 4, No. 2, 301, 1908.